Journal of Alloys and Compounds 509 (2011) 4816–4823

Contents lists available at ScienceDirect

Journal of Alloys and Compounds

journal homepage: www.elsevier.com/locate/jallcom

Doping and annealing effects on ZnO:Cd thin films by sol–gel method

Gang Li[a], Xuebin Zhu[a,*], Xianwu Tang[a], Wenhai Song[a], Zhaorong Yang[a], Jianming Dai[a], Yuping Sun[a], Xu Pan[b], Songyuan Dai[b]

[a] Key Laboratory of Materials Physics, Institute of Solid State Physics, Chinese Academy of Sciences, Hefei 230031, PR China
[b] Key Laboratory of New Thin Film Solar Cells, Institute of Plasma Physics, Chinese Academy of Sciences, Hefei 230031, PR China

ARTICLE INFO

Article history:
Received 26 June 2010
Received in revised form 4 January 2011
Accepted 30 January 2011
Available online 22 February 2011

Keywords:
ZnO:Cd
Transparent conductive oxide
Sol–gel

ABSTRACT

In this article, ZnO:Cd films were successfully deposited on glass substrates by a sol–gel technique. The influence of doping concentration and annealing temperature effects was carefully investigated. All films exhibited *c*-axis preferential orientation and optical transparency with visible transmittance >80%. The minimum room temperature resistivity of 0.0341 Ω cm was obtained with 10 at.% Cd doping under 600 °C annealing temperature. The optical band gap of ZnO:Cd film was reduced as Cd doping concentration increased, while the band gap increased with the increase of annealing temperature.

1. Introduction

In recent years, transparent conducting oxides (TCOs) have received much attention on their wide applications in the fields of optoelectronic devices. With a high thermal stability [1], good resistance against hydrogen plasma processing damage and low cost [2–4], zinc oxide is considered as one of the most promising TCOs which has been applied in light-emitting diodes, window materials in solar cells, liquid crystal displays and so on [5–7].

The possibility of practical applications of any TCOs relies on the potent manipulation of their physical properties. Impurity doping is necessary for a successful manipulation of the physical properties. Considerable works have been reported on the doping of ZnO with several dopants to tailor its electrical and optical properties [8–11]. Band gap engineering is essential to fabricate optical devices. The incorporation of Cd into ZnO is found to be useful for the realization of heterojunction and superlattice structures.

Various deposition techniques have been employed to fabricate ZnO:Cd thin films or nanoparticles, such as electro-deposition [12], pulsed laser deposition [13], molecular-beam epitaxy [14], sol–gel process [15,16] and so on. Zhang et al. [17] examined the effect of rapid thermal annealing (RTA) on crystal structures of ZnO:Cd films derived from reactive direct-current magnetron sputtering. It was found that for the $Zn_{0.9}Cd_{0.1}O$ films, they maintained single hexagonal phase when subjected to the RTA at 500–700 °C, while for the $Zn_{0.48}Cd_{0.52}O$ films, they were transformed into hexagonal and cubic phases when subjected to the RTA. Lee et al. [13] studied the effect of chemical composition on the optical properties of ZnO:Cd films deposited by the PLD method. As the deposition temperature decreased, the average transmittance decreased accompanied by a shift of absorption edge to the longer wavelength, which was mainly attributed to the change of Cd/Zn ratio. Mahmoud et al. [18] reported the influence of temperature on the structure of Cd-doped ZnO nanopowders prepared by the sol–gel method. The structure of ZnO:Cd nanopowder was changed from binary mixture to a single hexagonal phase when the annealing temperature increased above 400 °C.

The sol–gel process has been widely used for preparing nanostructured films of different materials and devices, which is considered as a facile route for a large-area coating at relatively low temperature and low cost. The properties of sol–gel derived ZnO:Cd thin films are generally affected by the preparation conditions including starting materials, sol concentration, thermal treatment temperature, and so on. Vijayalakshmi et al. [19] studied the influence of doping concentration on ZnO:Cd films, with the finding that the near band edge (NBE) emission showed a redshift which indicated the narrowing of the band gap due to Cd incorporation. Vigil et al. [20] reported the effect of annealing time on ZnO:Cd films. The defect concentration in the film appeared to be reduced as revealed by a smaller band tailing parameters when the annealing time increased. There are lots of sol–gel papers focus on ZnO:Cd films up to now, however, the discussion about the influence of annealing temperature on ZnO:Cd films is seldom. Therefore, this article conducts an investigation into the effects of doping concentration and annealing temperature on the structural, morphological, optical and electrical properties for sol–gel derived ZnO:Cd thin films.

* Corresponding author.
E-mail address: xbzhu@issp.ac.cn (X. Zhu).

0925-8388/$ – see front matter © 2011 Elsevier B.V. All rights reserved.
doi:10.1016/j.jallcom.2011.01.176

The results show that the preparation conditions play a very obvious role in the properties of ZnO:Cd films.

2. Experimental procedure

ZnO:Cd thin films were prepared via sol–gel method. At first, $Zn(CH_3COO)_2{\cdot}2H_2O$ was added into a mixture of 2-methoxyethanol and monoethanolamine (MEA). The molar ratio of MEA to zinc acetate was maintained at 1.0, and the concentration of zinc acetate was 0.4 M. Then $Cd(CH_3COO)_2{\cdot}2H_2O$ was added into the solution with the Cd/Zn nominal ratio of 0, 5, 10, 20 and 30 at.%. The solution was stirred at room temperature for more than 4 h in order to get a well-mixed precursor solution.

Before deposition, glass substrates were cleaned with acetone, ethanol and deionized water successively in an ultrasonic bath. The films were deposited with a spin coater at the rotating speed of 5000 rpm for 20 s. After each coating, the as-deposited films were dried at 300 °C in air for 15 min to evaporate the organics. The procedures from coating to drying were repeated for six times to increase the thickness. Then, the films were inserted into a tube furnace and heated at 450–600 °C in air for 1 h. Finally, all the films were annealed in N_2 atmosphere for 1 h in order to enhance their electrical conductivity. A warming temperature speed was 10 °C/min and a natural cooling was maintained after finishing the annealing.

X-ray diffraction (XRD) using a Philips X'pert Pro diffractometer with Cu K_α radiation was carried out to check up the crystal structure. The surface and cross section of the films were observed by field-emission scanning electronic microscopy (FE-SEM, FEI Sirion 200 type). The thickness of the film was evaluated from FE-SEM image of the cross section of the film. Optical transmittance of the derived films was measured using an automated scanning monochromator (Varian-designed Cary-5E type). The measurement was performed using air as reference in a wavelength range of 200–600 nm. The electrical resistance was measured by a physical properties measurement system (PPMS, Quantum-designed) via the standard four-point probe method.

3. Results and discussion

3.1. The effects of the doping concentration

Fig. 1 shows the XRD patterns of ZnO:Cd ($0 \leq Cd/Zn \leq 30$ at.%) films at different doping concentrations. All the peaks match the hexagonal ZnO structure, without the evidence of the peaks corresponding to either cadmium, zinc or their complex oxides. Moreover, despite the amorphous native surfaces of the glass substrates, all films exhibit *c*-axis preferential orientation which results from the self-ordering effect caused by the minimization of crystal surface free energy [21]. Nucleation with various orientations can be formed at initial stage. Though all nuclei compete to grow, only nuclei having the lowest surface free energy can survive, i.e., *c*-axis orientation is achieved. However, the Cd content leads to a change in the XRD intensity, and 10 at.% cadmium-doped film has the strongest XRD intensity of the (0 0 2) peak. At low doping concentration, the increase in the (0 0 2) peak may be attributed to the formation of new nucleating centers due to dopant atoms resulting from the decrease of nucleation energy barrier [22]. The subsequent decrease of (0 0 2) peak intensity for higher doping concentration may be affected by the saturation of newer nucleating centers [22,23] and the segregation of amorphous cadmium components. Ohyama et al. [24] studied the effect of aluminum content on the structure of ZnO:Al films, and thought the decrease of (0 0 2) peak could be due to the segregation of aluminum components at the grain boundary for the higher aluminum content, though no impurity phases were found from the XRD patterns [24].

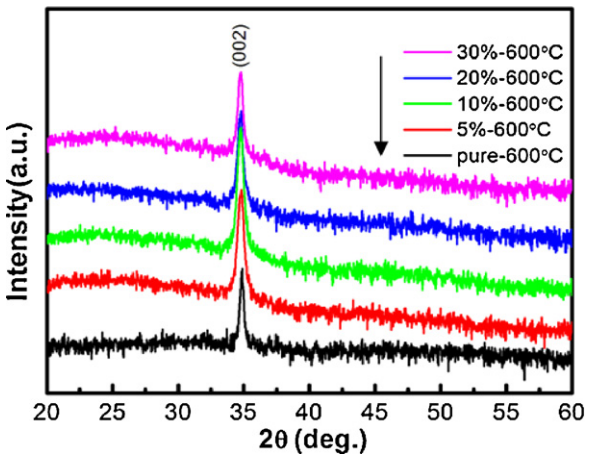

Fig. 1. XRD patterns of ZnO:Cd thin films with different doping concentrations.

Fig. 2 shows the surface morphologies and the cross sectional FE-SEM micrographs of ZnO:Cd films with different doping concentrations. All films exhibit homogeneous surface covered with many small grains, and inter-grain connection is developed. It is evident that those voids in the films increase with the rise of doping level. All films have a similar grain size of ~40–50 nm, and the doping concentration has no obvious effect on the grain size. This phenomenon could be explained from the following aspects: on one hand, the grain size would decrease due to the increase of the

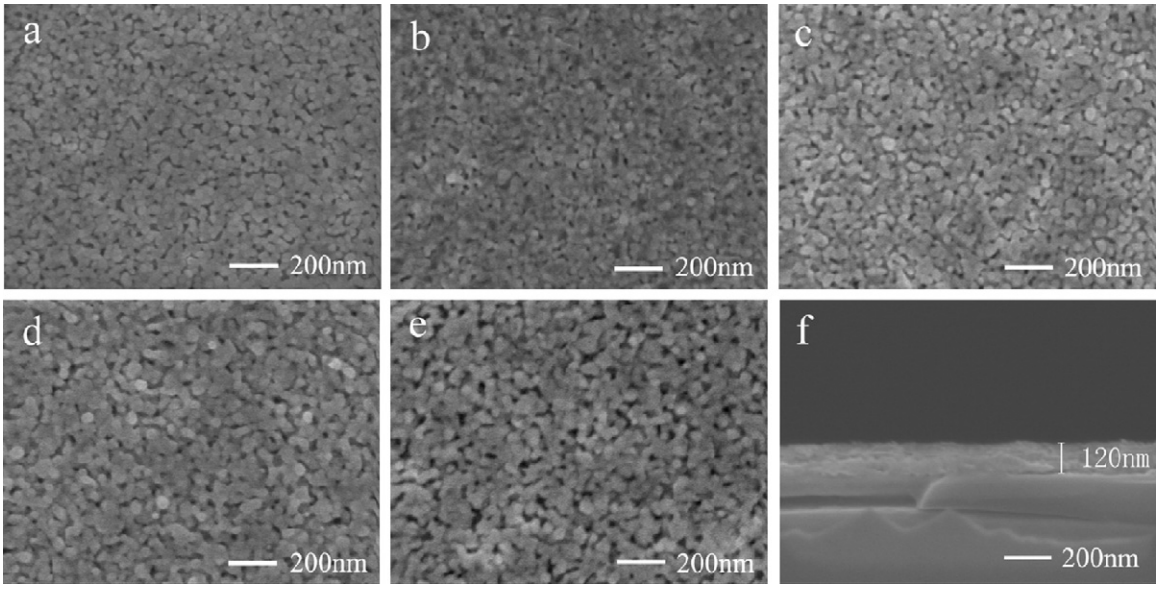

Fig. 2. FE-SEM micrographs of the surface and the cross section of ZnO:Cd thin films for doping concentration of (a) 0 at.%, (b) 5 at.%, (c) 10 at.%, (d) 20 at.%, and (e) 30 at.%.

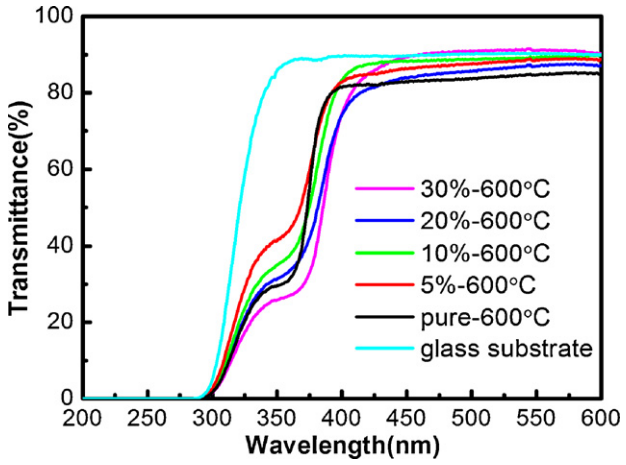

Fig. 3. The transmission spectra of ZnO:Cd thin films with different doping concentrations.

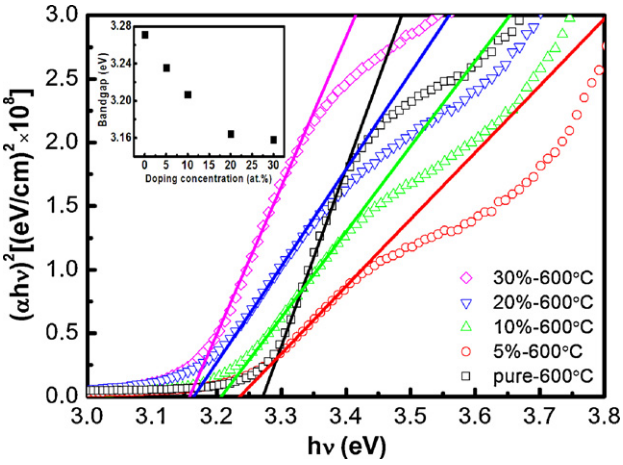

Fig. 4. $(\alpha h\nu)^2$ versus $h\nu$ plot of ZnO:Cd thin films with different doping concentrations. The inset shows band gap energy as a function of Cd doping concentration.

dopant atoms, which can exert a drag force on boundary motion and grain growth [25]; on the other hand, higher doping concentration can simultaneously lead to the increased point defect concentrations, which would give rise to higher grain boundary mobility and grain growth rate [25] and make the grain size larger. These two competitive effects will lead to the slight change of the grain size. The cross sectional micrograph of ZnO:Cd film with doping concentration of 10 at.% is shown in Fig. 2(f). Though the doping concentration is different, it is observed that the thicknesses of all films are approximately 120 nm owing to the same preparation conditions.

Fig. 3 shows the optical transmission of ZnO:Cd films with different doping concentrations. The decrease in the transmission at about 290–340 nm is owing to the absorption of glass substrates. The optical transmission of all the films is over 80% in the visible region of 400–600 nm, which reveals that the films are highly transparent in the visible region. Additionally, it seems that the influence of doping concentration on the transmittance spectra is random. However, there is a visible change in the band gap absorption edge of ZnO:Cd thin films. The absorption edge of undoped ZnO film is sharp while that of ZnO:Cd film is relatively wide. The absorption coefficient (α) was calculated using Manifacier model [26]. The dependence of α on the photon energy ($h\nu$) was fitted to the relation [27]:

$$\alpha h\nu = A(h\nu - E_g)^n$$

where A is a constant, E_g represents the optical band gap while the exponent n depends on the type of the transition. For direct allowed transition, indirect allowed transition and direct forbidden transition, n equals to 1/2, 2 and 3/2, respectively. Both ZnO and CdO are considered as materials with direct band gap energy [28]. Extrapolation of the linear portion of the plots of $(\alpha h\nu)^2$ versus $h\nu$ to $\alpha = 0$ gives the optical band gap of the films for direct allowed transition. The plot of $(\alpha h\nu)^2$ versus $h\nu$ of ZnO:Cd films deposited at different doping concentrations is shown in Fig. 4. Apparently, as the optical band gap decreases from 3.27 eV to 3.16 eV (shown in the inset of Fig. 4), the optical absorption edge exhibits a red-shift with the rise of Cd doping concentration from 0 to 30 at.%. The narrowing band gap is due to the existence of Cd impurities in the ZnO structure, which induce the formation of new recombination centers with lower emission energy [16]. Ma et al. [29] reported ZnO:Cd films with a similar E_g value, but Vijayalakshmi et al. [19] observed a smaller E_g value ~2.96 eV of ZnO:Cd film derived from spray pyrolysis method. The difference in results may be related to the preparation technology, which leads to the variation of defects types and concentration. Zhang et al. [30] performed a first-principles study and employed the Perdew–Burke–Ernzerhof form of the generalized gradient approximation to evaluate the electronic and optical properties of ZnO:Cd. They obtained that with increasing Cd concentrations, the band gap of ZnO:Cd was decreased due to the increase of s states in the conduction band. Tang et al. [31] applied first-principles calculation with the PAW-GGA method to study wurtzite $Zn_{1-x}Cd_xO$ alloys. They attributed the reduction of band gap with the increase of Cd content to the contributions of the hybridization of electronic states of Zn-4s and Cd-5s, the enhancement of p–d repulsion and the tensile strain due to Cd-doping.

The temperature dependence of resistivity ρ–T of ZnO:Cd thin films with different doping concentrations is shown in Fig. 5. It can be seen that all films exhibit semiconductive behaviors. Table 1 shows the room temperature (RT) resistivity of several typical ZnO:Cd thin films. It can be observed that the RT resistivity decreases gradually with the increase of Cd concentration up to 10 at.%, which shows the minimum of 0.0341 Ω cm; however, with further doping concentration, the RT resistivity reverts to increase. The lowest RT resistivity of 10 at.% Cd-doped film can be attributed to the enhancement of crystallization quality [24]. Due to the isovalent ions of Cd^{2+} and Zn^{2+}, there is no contribution of extra free charge carriers from the substitution. At low doping concentration, the higher crystal orientation can be thought to reduce the resistivity, because the charge carrier mobility will increase due to the

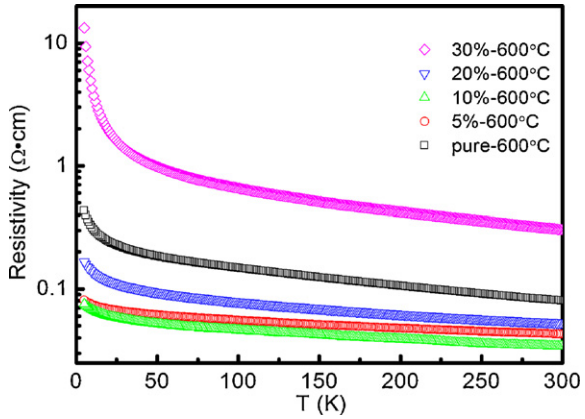

Fig. 5. Temperature dependence of the resistivity for ZnO:Cd thin films with different doping concentrations.

Table 1
Comparison of room temperature (300 K) resistivity and thermal activation energy between some ZnO:Cd thin films.

Sample	Doping concentration (at.%)	Annealing temperature (°C)	Room temperature resistivity (Ω cm)	Thermal activation energy (meV)
1	0	600	0.0805	12.4
2	5	600	0.0429	5.6
3	10	600	0.0341	5.5
4	20	600	0.0535	7.1
5	30	600	0.3054	18.3
6	10	450	0.1195	7.0
7	10	500	0.0472	6.8
8	10	550	0.0356	6.7
9	20	450	0.9843	24.2
10	20	500	0.2234	11.9
11	20	550	0.0744	8.7

shorter carrier path length in a *c*-plane and the reduction in the scattering of the charge carriers at the crystal defects [24]. However, the resistivity gradually increases as the dopant level gets a further increase. Higher level of cadmium incorporation leads to interstitial incorporation of Cd that gives rise to greater electron scattering. Meanwhile, The cadmium atoms may also segregate at the grain boundaries in the form of amorphous cadmium components, which will increase the grain boundary barrier [32]. Thus, the mobility of charge carrier decreases as more scattering and grain boundary barrier effects occur. The resistivity of ZnO:Cd film with 30 at.% of cadmium is evidently higher than those of the other films, which may result from the enhanced scattering at grain boundary micropores (as shown in Fig. 2).

In order to further study the transport properties of ZnO:Cd film, the ρ–T results were fitted with different models. As a typical example, Fig. 6 shows the ρ–T fitting of 30% Cd-doped ZnO film. The thermal activation model, $\rho \sim \exp(T_0/T)$ where T_0 is the activation energy, can only be well fitted within the temperature range of 200–300 K, whereas at lower temperatures the variable range hopping (VRH) model, $\rho \sim \exp(T_0/T)^{1/4}$, is suitable. Table 1

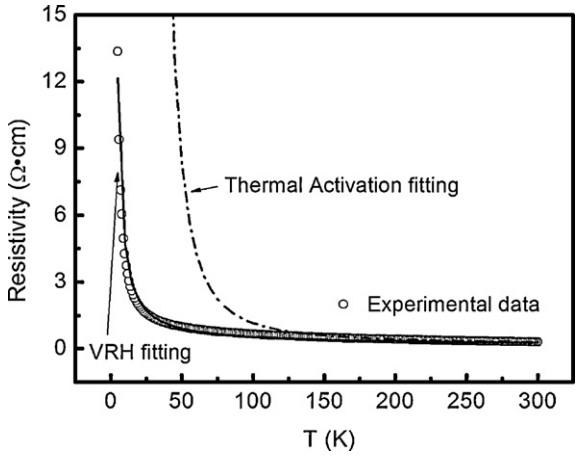

Fig. 6. ρ–T fitting results for 30% Cd-doped ZnO film.

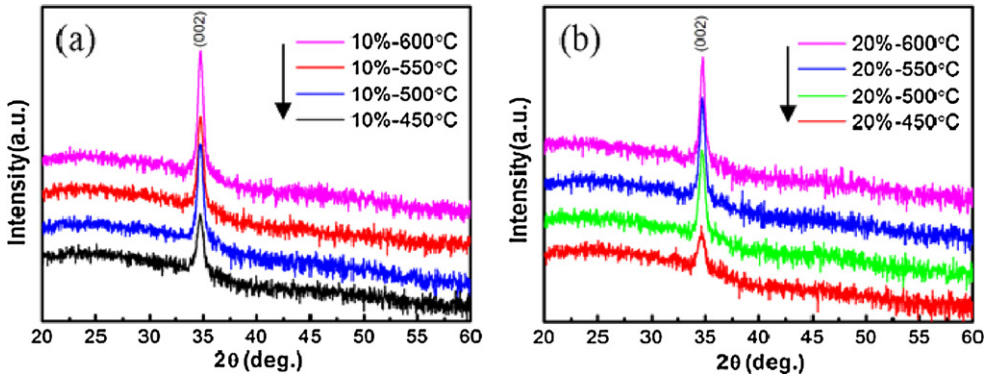

Fig. 7. XRD patterns of ZnO:Cd thin films with different annealing temperatures in air.

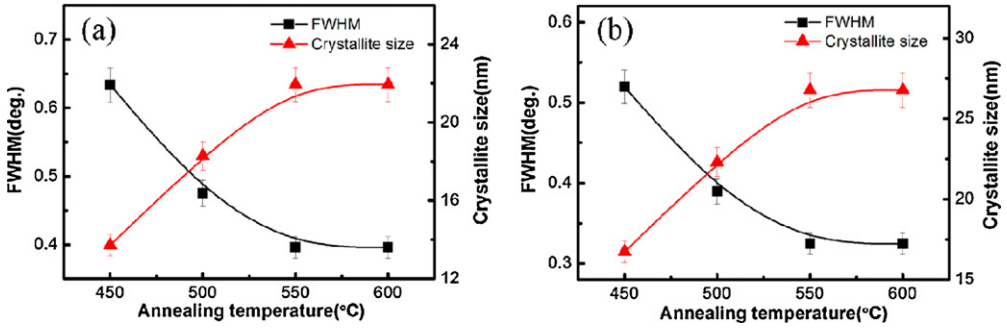

Fig. 8. Variation of FWHM and the crystallite size of ZnO:Cd thin films with different annealing temperatures in air at doping concentration of (a) 10% and (b) 20%.

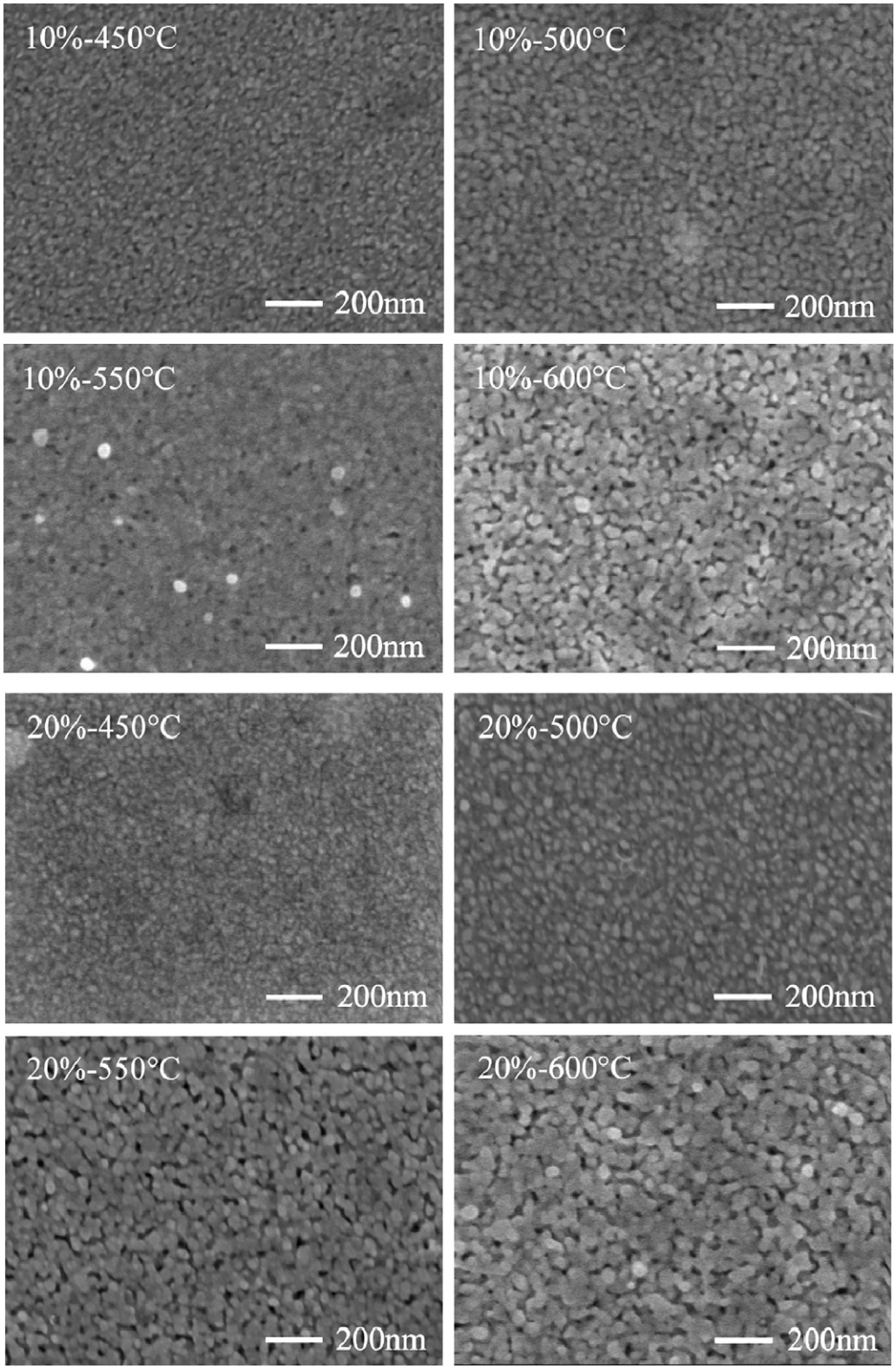

Fig. 9. FE-SEM micrographs of ZnO:Cd thin films with different annealing temperatures in air.

shows the fitting thermal activation energy of ZnO:Cd films with different doping concentrations. It can be seen that the change of thermal activation energy is corresponding to that of the resistivity. The smallest activation energy of 10% Cd-doped ZnO film indicates that it has a relatively higher charge carrier mobility, which further demonstrates the validity of the above analysis of resistivity.

3.2. The effects of the annealing temperature

The XRD patterns of ZnO:Cd thin films annealed in different temperatures in air are shown in Fig. 7. Only ZnO (0 0 2) peak is observed in the scanning range of 20–60 for all samples. The intensity of (0 0 2) peak increases with the rise of annealing temperature, indi-

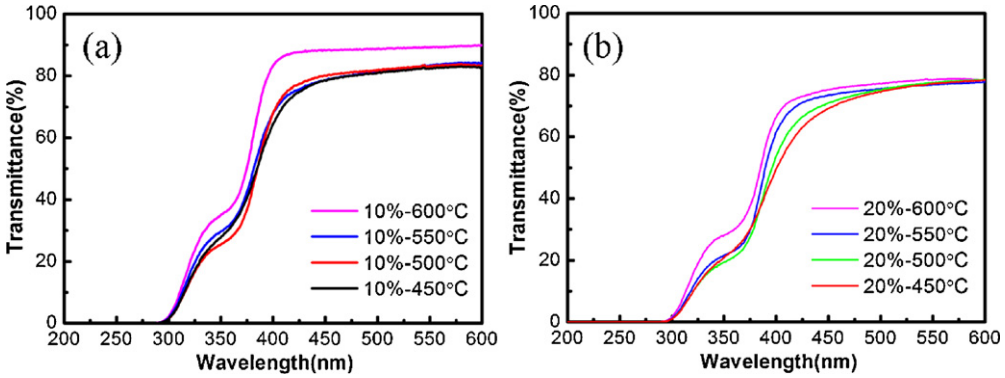

Fig. 10. Transmission spectra of ZnO:Cd thin films with different annealing temperatures in air.

cating the improved crystallinity of the derived films. Many groups reported the influence of annealing temperature on the structural property of ZnO thin films. They thought the improvement of crystallinity was due to the relief of the stress as annealing temperature increases [33–35]. The stress is composed of a thermal stress and an intrinsic stress. The thermal stress is due to the difference in the thermal expansion coefficients of the film and substrate. The intrinsic stress is due to the incorporation of defects. It is noted that the peak position (2θ) corresponding to (0 0 2) reflection for all the films is less than that for unstressed ZnO powder (not shown here). The lower value of 2θ indicates that the films are in a state of uniform compressive stress. Increasing annealing temperature, the 2θ value shifts towards a high angle, which means the compressive stress has been relieves because the defects of the film will be decreased [34]. Another reason is that the thermal expansion coefficient of ZnO ($7 \times 10^{-6}/^{\circ}C$) is bigger than that of glass ($4.6 \times 10^{-6}/^{\circ}C$), a tensile stress is given for glass substrate [36].

Fig. 8 shows the full width at half maximum (FWHM) of (0 0 2) peak and the crystallite size of ZnO:Cd thin films with different annealing temperatures in air. The crystallite size can be calculated with Scherrer's equation [37]:

$$D = \frac{K\lambda}{\beta \cos \theta}$$

where λ is the X-ray wavelength, θ is the Bragg diffraction angle, β is the FWHM of θ, and K (usually nearly 1) is a correction factor. It is observed that as annealing temperature increases, the FWHM value decreases whereas the crystallite size increases, which is attributed to the enhanced atomic diffusion [25]. The result suggests that the crystallization quality of ZnO:Cd thin films may be improved with the rise of annealing temperature in air. Moreover, when annealing temperature goes beyond 550 °C, a tendency to saturation has been detected. With further increase of annealing temperature, the cadmium atoms tend to segregate to grain boundaries, which may exert a drag force on boundary motion to hamper the crystallite growth [25]. From the comparison of crystallite size at same annealing temperature but different Cd concentration as shown in the Fig. 8(a) and (b), it is clear that the crystallite size enlarges with increasing doping concentration. Considering that the ionic radius of Cd^{2+} is larger than that of Zn^{2+}, this partly explains that the substitution of Zn with Cd takes place on the equivalent crystallographic position of Zn in hexagonal wurtzite structure [29].

The surface morphologies of ZnO:Cd films at various annealing temperatures in air are shown in Fig. 9. A strong influence of annealing temperature on the grain growth can be clearly detected. The grains grow to larger sizes as annealing temperature in air rises from 450 to 600 °C, which is attributed to the enhancement of atomic diffusion [25]. However, these grains have larger average sizes compared with that obtained via XRD analysis in the present study, which indicates that the grains are composed of several crystallites [38]. Moreover, as annealing temperature increases, the inter-grain connection gets developed and the grain boundary micropores turn clearer, which result from coarsening during coalescence.

Fig. 10 shows the optical transmittance spectra of ZnO:Cd films at different annealing temperatures in air. Although the dependence of the transmission in the visible region on annealing temperature is random, it seems that the film annealed at 600 °C has a higher transmission, which indicates the crystallization quality effects on the optical properties. Additionally, it can be seen that the variation of the optical absorption edge is apparent in Fig. 10. In order to show this effect, the absorption has been inves-

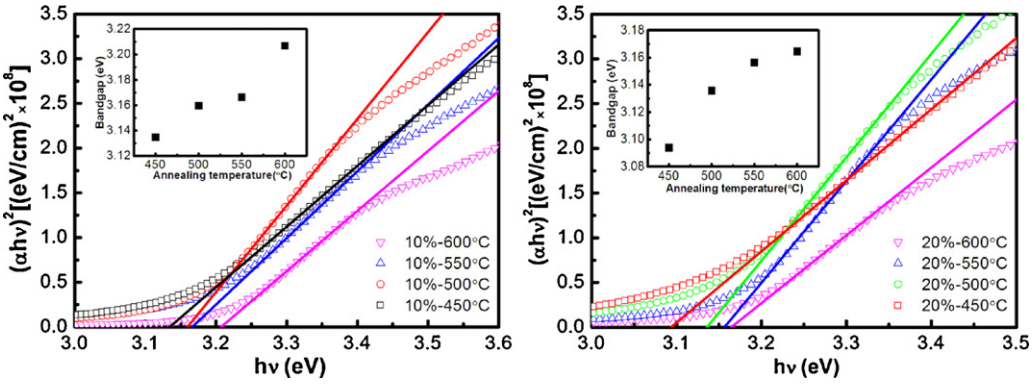

Fig. 11. $(\alpha h\nu)^2$ versus $h\nu$ plot of ZnO:Cd thin films with different annealing temperatures in air. The inset shows band gap energy as a function of annealing temperature in air.

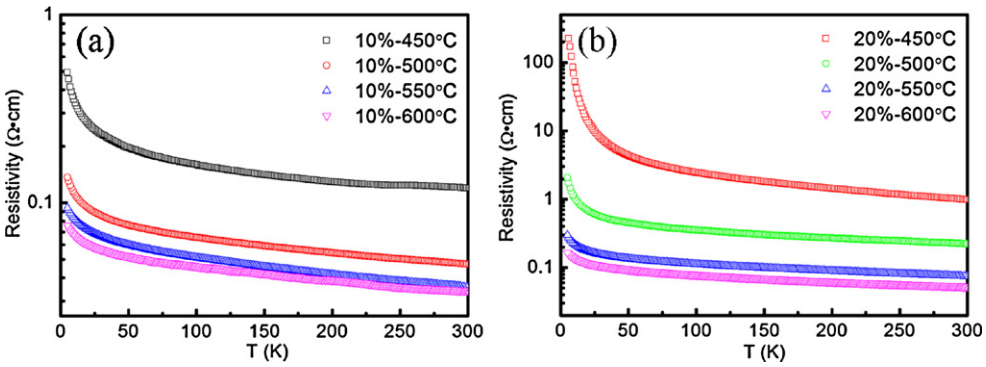

Fig. 12. Temperature dependence of the resistivity for ZnO:Cd thin films with different annealing temperatures in air.

tigated for the film annealed at different annealing temperatures in air. Fig. 11 shows the plot of $(\alpha h\nu)^2$ versus $h\nu$ of ZnO:Cd films with different annealing temperatures in air. The optical absorption edge shifts to a short wavelength with increasing annealing temperature in air. This blueshift can be explained by several mechanisms: one is the result of the Burstein–Moss effect [39]. This originates from the motion of Fermi level owing to an increase in the charge carrier concentration as annealing temperature rising. Another is attributed to the decrease in shallow-level trap concentration near the conduction band of ZnO:Cd thin film resulting from the enhancement of crystallinity [40] as shown in Fig. 7. Dutta et al. [41] and Srikant et al. [42] have reported the enhancement band gap with the increase of grain size in ZnO nanoparticles. In nanocrystalline materials the surface to volume ratio gets so high that band bending can be expected at the grain boundaries. In smaller grains, the band bending effect is greater and the band edge becomes flatter than that of larger grains. In this present work, the grains grow to larger sizes as annealing temperature increases (shown in Fig. 9), hence the observed blueshift can also be attributed to the reduction of band bending effect at the grain boundaries [41–43].

Fig. 12 shows the temperature dependence of the resistivity for ZnO:Cd thin films at different annealing temperatures in air. It is also semiconductive for all films. Clearly, in Table 1, the RT resistivity of ZnO:Cd films with same doping concentration goes downward as annealing temperature rising, and the film annealed at 600 °C shows the minimum resistivity value. In fact, the resistivity is determined by charge carrier concentration and mobility. On one hand, the grain boundaries and the crystal lattice deficiencies of the film due to the defects such as interstitial oxygen are decreased with the increase of annealing temperature [44], which cause an increase of the charge carrier concentrations. Meanwhile, the film with larger grain size has higher charge carrier concentrations, which result from the grain boundary barrier effect [45]. Therefore, the charge carrier concentrations increase with annealing temperature. On the other hand, the rise of annealing temperature leads to an enhancement of crystallinity, which minimizes the concentration of shallow-level trap. The growth of grain size brings about the decrease in the grain boundaries density (as shown in Fig. 9). The mobility of charge carriers is enhanced by the decrease of electron scattering, which are caused by shallow-level trap and the grain boundaries. Consequently, these two factors gives rise to the decrease in RT resistivity [40,46].

The ρ–T results were also fitted with the thermal activation model and the VRH model. The fitting thermal activation energy of ZnO:Cd films at different annealing temperatures in air are shown in Table 1. It can be seen that the thermal activation energy diminishes as annealing temperature in air increases, which may result from the enhanced electron activation from a donor due to the higher crystal-quality.

4. Conclusion

ZnO:Cd films were successfully deposited on glass substrates via the sol–gel method. The influences of doping concentration as well as annealing temperature in air on the structural, morphology, electrical and optical characteristics have been investigated. The results are summarized as follows:

(1) All films exhibit *c*-axis preferential orientation and optical transparency with visible transmittance >80%.
(2) Doping concentration plays a subtle role in determining the grain growth, while the increase of annealing temperature in air can lead to the growth of grain size.
(3) The optical band gap of ZnO:Cd film is gradually diminished as Cd doping concentration increases, while the band gap increases with rising annealing temperature in air.
(4) Due to the enhancement in crystallization quality and the growth of grain size, the film with Cd concentration of 10% under annealing temperature of 600 °C exhibits the minimum resistivity of 0.0341 Ω cm.

The results indicate that the optical band gap and electrical conductivity for ZnO:Cd films could be simultaneously tuned by changing the doping concentration and annealing temperature.

Acknowledgements

This work was supported by the National Key Basic Research under Contract No. 2007CB925002, and the National Nature Science Foundation of China under Contract Nos. 10774146 and 50802096, Anhui Province NSF Grant No. 070414162, and Director's Fund of Hefei Institutes of Physical Science, Chinese Academy of Sciences.

References

[1] K.Y. Wu, C.C. Wang, D.H. Chen, Nanotechnology 18 (2007) 305604.
[2] J.H. Lee, B.O. Park, Thin Solid Films 426 (2003) 94.
[3] J. Herrero, C. Guillen, Thin Solid Films 451/452 (2004) 630.
[4] D. Basak, G. Amin, B. Mallik, G.K. Paul, S.K. Sen, J. Cryst. Growth 256 (2003) 73.
[5] K. Minegishi, Y. Koiwai, Y. Kikuchi, K. Yano, Jpn. J. Appl. Phys. Part 2 36 (1997) L1453.
[6] D.C. Look, Mater. Sci. Eng. B 80 (2001) 383.
[7] K.L. Chopra, S. Major, D.K. Pandya, Thin Solid Films 102 (1983) 1.
[8] P. Wang, N.F. Chen, Z.G. Yin, F. Yang, C.T. Peng, J. Cryst. Growth 290 (2006) 56.
[9] F. Ran, L. Miao, S. Tanemura, M. Tanemura, Y. Cao, S. Tanaka, N. Shibata, Mater. Sci. Eng. B 148 (2008) 35.
[10] L.H. Xu, X.Y. Li, J. Yuan, Superlattices Microstruct. 44 (2008) 276.
[11] K. Yoshino, S. Oyama, M. Yoneta, J. Mater. Sci: Mater. Electron. 19 (2008) 203.
[12] M. Tortosa, M. Mollar, B. Mari, J. Cryst. Growth 304 (2007) 97.
[13] S.Y. Lee, Y. Li, J.S. Lee, J.K. Lee, M. Nastasi, S.A. Crooker, A.X. Jia, H.S. Kang, J.S. Kang, Appl. Phys. Lett. 85 (2004) 2.
[14] K. Sakurai, T. Takagi, T. Kubo, K. Kajita, T. Tanabe, H. Takasu, S. Fujita, J. Cryst. Growth 514 (2002) 237.
[15] Y. Caglar, M. Caglar, S. Ilican, A. Ates, J. Phys. D: Appl. Phys. 42 (2009) 065421.

[16] F. Yakuphanoglu, S. Ilican, M. Caglar, Y. Caglar, Superlattices Microstruct. 47 (2010) 732.
[17] R.J. Zhang, P.L. Chen, Y.Y. Zhang, X.Y. Ma, D.R. Yang, J. Cryst. Growth 312 (2010) 1908.
[18] W.E. Mahmoud, A.A. Al-Ghamdi, S. Al-Heniti, S. Al-Ameer, J. Alloys Compd. 491 (2010) 742.
[19] S. Vijayalakshmi, S. Venkataraj, R. Jayavel, J. Phys. D: Appl. Phys. 41 (2008) 245403.
[20] O. Vigil, F. Cruz, G. Santana, L. Vaillant, A. Morales-Acevedo, G. Contreras-Puente, Appl. Surf. Sci. 161 (2000) 27.
[21] X. Jiang, C.L. Jia, R.J. Hong, J. Cryst. Growth 289 (2006) 464.
[22] M. Öztas, M. Bedir, Thin Solid Films 516 (2008) 1703.
[23] G. Li, X.B. Zhu, H.C. Lei, W.H. Song, Z.R. Yang, J.M. Dai, Y.P. Sun, X. Pan, S.Y. Dai, J. Alloys Compd. 505 (2010) 434.
[24] M. Ohyama, H. Kozuka, T. Yoko, J. Am. Ceram. Soc. 81 (1998) 1622.
[25] C.V. Thompson, Annu. Rev. Mater. Sci. 20 (1990) 245.
[26] J.C. Manifacier, J. Gasiot, J.P. Fillard, J. Phys., E. J. Sci. Instrum. 9 (1976) 1002.
[27] E. Ziegler, A. Heinrich, H. Oppermann, G. Stover, Phys. Status Solidi A 66 (1981) 635.
[28] H. Tabet-Derraz, N. Benramdane, D. Nacer, A. Bouzidi, M. Medles, Sol. Energy Mater. Sol. Cells 73 (2002) 249.
[29] D.W. Ma, Z.Z. Ye, J.Y. Huang, L.P. Zhu, B.H. Zhao, J.H. He, Mater. Sci. Eng. B 111 (2004) 9.
[30] X.D. Zhang, M.L. Guo, W.X. Li, C.L. Liu, J. Appl. Phys. 103 (2008), 063721.
[31] X. Tang, H.F. Lu, J.J. Zhao, Q.Y. Zhang, J. Phys. Chem. Solids 71 (2010) 336.
[32] M.J. Alam, D.C. Cameron, J. Vac. Sci. Technol. A 19 (2001) 1642.
[33] M.L. Cui, X.M. Wu, L.J. Zhuge, Y.D. Meng, Vacuum 81 (2007) 899.
[34] W. Water, S.Y. Chu, Mater. Lett. 55 (2002) 67.
[35] H.K. Yadav, K. Sreenivas, V. Gupta, J. Appl. Phys. 99 (2006) 083507.
[36] H. Kim, J.S. Horwitz, S.B. Qadri, D.B. Chrisey, Thin Solid Films 420/421 (2002) 107.
[37] B.D. Cullity, S.R. Stock, Elements of X-ray Diffraction, 3rd edition, Prentice Hall, New Jersey, 2001.
[38] M. Bouderbala, S. Hamzaoui, B. Amrani, A.H. Reshak, M. Adnane, T. Sahraoui, M. Zerdali, Physica B 403 (2008) 3326.
[39] B.E. Sernelius, K.F. Berggren, Z.C. Jin, I. Hamberg, C.G. Granqvist, Phys. Rev. B 37 (1988) 10244.
[40] J.P. Lin, J.M. Wu, Appl. Phys. Lett. 92 (2008) 134103.
[41] S. Dutta, S. Chattopadhyay, M. Sutradhar, A. Sarkar, M. Chakrabarti, D. Sanyal, D. Jana, J. Phys. Condens. Matter. 19 (2007) 236218.
[42] V. Srikant, D.R. Clark, J. Appl. Phys. 81 (1997) 6357.
[43] R. Vinodkumar, K.J. Lethy, P.R. Arunkumar, R.R. Krishnan, N.V. Pillai, V.P.M. Pillai, R. Philip, Mater. Chem. Phys. 121 (2010) 406.
[44] H.M. Zhou, D.Q. Yi, Z.M. Yu, L.R. Xiao, J. Li, Thin Solid Films 515 (2007) 6909.
[45] Y.Q. Zhou, I. Matsubara, W. Shin, N. Izu, N. Murayama, J. Appl. Phys. 95 (2004) 625.
[46] M. Bouderbala, S. Hamzaoui, B. Amrani, H. Ali, M. Reshak, T. Adnane, M. Sahraoui, Zerdali, Physica B 403 (2008) 3326.